Novel method for selecting the regions of interest in hyperspectral images of apples with random poses on the sorting line

Kangkang Qi[1], Wenbin Wu[2], Shuai Wang[1], Yuanjie Mu[1], Qian Song[2], Fengyun Wang[1*], Yangyang Fan[1], Wenjie Feng[1*], Rui Li[3], Longsheng Fu[3*]

(1. *Agricultural Information and Economy Institution, Shandong Academy of Agricultural Sciences, Jinan 250100, China*;
2. *State Key Laboratory of Efficient Utilization of Arid and Semi-arid Arable Land in Northern China, Institute of Agricultural Resources and Regional Planning, Chinese Academy of Agricultural Sciences, Beijing 100081, China*;
3. *College of Mechanical and Electronic Engineering, Northwest A & F University, Yangling 712100, Shaanxi, China*)

Abstract: Recent approaches to the internal quality inspection of apples with the application of hyperspectral imaging technology are highly cost-intensive because of labor involvement for the data collection on a fixed posture and manual selection of the region of interest (RoI). In addition, several studies have repeated the data acquisition for the same apple. Current methods cannot meet the automation requirements of the sorting line. Therefore, this study proposed a novel method for automatically selecting RoI in hyperspectral images of apples with random poses. Firstly, the preliminary RoI selection of apple hyperspectral image was carried out, followed by the performance of histogram statistics of each pixel with spectral intensity at 700 nm wavelength. The top 40% area of the spectral intensity was reserved to obtain the magnitude relationship of the spectral intensity of each pixel point and a morphological erosion operation. Original apple RoI was acquired and overexposed pixels were removed with spectral intensity greater than 3900 (maximum 4095) in the reserved area at 700 nm. Secondly, the relationship between apple size and prediction accuracy was measured for the in-depth RoI analysis. A partial least square regression (PLSR) model was established between the average spectrum and apple sugar content of RoI with different sizes. Finally, the established model with the top 70% of the spectral intensity achieved the best prediction accuracy. Non-destructive estimation of apple sugar content was performed through hyperspectral imaging technology with reference to the proposed RoI selection method. A competitive adaptive reweighted sampling algorithm along the PLSR (CARS-PLSR) model was established after black-and-white correction and standard normal transformation (SNV) preprocessing and obtained the highest prediction accuracy. The determination coefficient of cross-validation (R_{cv}) and root mean square error of cross-validation (RMSECV) were 0.9595 and 0.3203°Brix, respectively. The determination coefficient of prediction (R_p) was 0.9308, and the root mean square error of prediction (RMSEP) was 0.4681°Brix. Results proved that the auto-selection of RoI is an efficient and accurate method, which can provide a foundation in practical application for online apple grading systems with hyperspectral imaging technology.

Keywords: apple, hyperspectral imaging, nondestructive detection, region of interest, sugar content
DOI: 10.25165/j.ijabe.20251801.9062

Citation: Qi K K, Wu W B, Wang S, Mu Y J, Song Q, Wang F Y, et al. Novel method for selecting the regions of interest in hyperspectral images of apples with random poses on the sorting line. Int J Agric & Biol Eng, 2025; 18(1): 199–207.

1 Introduction

Nowadays, hyperspectral imaging technology is used as a non-destructive detection system[1-3] and collects a large amount of data[4]. In non-destructive testing using hyperspectral imaging, region of interest (RoI) selection is an important step in model establishment[1] and provides the original characteristic of spectral data. RoI helps to obtain the average spectrum of RoI as the characteristic spectrum of the sample[5]. This process directly reduces the data size, which helps to decrease calculation complexities as well as improve the model establishment speed. Therefore, RoI selection of hyperspectral images is an important step in data analysis which influences the model accuracy.

Various researchers have explored hyperspectral imaging technology to determine internal fruit quality with different RoI selection methods[6-8]. Normally, in the hyperspectral imaging data collection stage, the imaging spectrometer is placed vertically at a 90° angle above the fruit with perpendicular movement. Xu et al.[9] detected apple quality by using photon transmission simulation and a convolutional neural network with a selected RoI of 40×40 pixels. In another study, the whole apple was chosen as RoI to determine its hardness[10]. To predict apple sugar content, Guo[11] used the light intensity correction method in hyperspectral visualization by selecting a circular area as RoI with a diameter of 150 pixels from

Received date: 2024-05-08 **Accepted date:** 2024-11-03
Biographies: Kangkang Qi, Assistant Researcher, research interest: modern agricultural equipment and agricultural big data, Email: qikangkang_vip@foxmail.com; **Wenbin Wu**, Researcher and Head, research interest: smart agriculture, wuwenbin@caas.cn; **Shuai Wang**, Associate Researcher, research interest: digital agriculture, Email: wangshuai@saas.ac.cn; **Yuanjie Mu**, Assistant Researcher, research interest: precision agriculture, Email: myj2437@163.com; **Qian Song**, Researcher, research interest: smart agriculture, Email: songqian01@caas.cn; **Yangyang Fan**, Assistant Researcher, research interest: plant phenotypomics, agricultural pest and disease detection, Email: fanyangy9836@163.com; **Rui Li**, Senior Experimentalist, research interest: smart agriculture, Email: ruili1216@nwafu.edu.cn.
***Corresponding author: Fengyun Wang**, Researcher, research interest: smart agriculture. No. 23788 Gongye North Road, Licheng District, Jinan, Shandong, China. Tel: +86-53166659241, Email: wfylily@163.com; **Wenjie Feng**, Researcher and Head, research interest: smart agriculture. No. 23788 Gongye North Road, Licheng District, Jinan, Shandong, China. Tel: +86-53166655246. Email: 34941269@qq.com; **Longsheng Fu**, Professor, research interest: smart agriculture, No. 22 Xinong Road, Yangling, Shannxi, China. Email: fulsh@nwafu.edu.cn.

the intersection of the apple pedicel-calyx connecting line and the equatorial plane. RoI is also manually selected and labeled for some prediction modeling. To avoid errors in manual labeling, there are a few certain rules in the selection of RoIs[12-14]. Zha[15] determined the soluble solids and hardness by rotating apples parallel with the core and collected hyperspectral data at every 120°. Three horizontal hyperspectral images were captured from one apple with a circular area (as RoI) with a 150-pixel radius. Then, the model was developed using the average spectrum of RoI as the characteristic spectrum. Feng et al.[16] focused on the soluble solid contents and collected hyperspectral data from two sides of apples by rotating it 180° along the core axis. The aim was to select four squared RoIs of 50 pixels with a 300-pixel distance from the central point from each side. A total of eight squared RoIs were obtained on both sides, and the average spectrum was indicated as a characteristic spectrum for modeling. Xu[17] collected a hyperspectral image from both (front and back) sides of each sample for the analysis of soluble solids in Dangshan pear. Furthermore, each collected image was normalized, and the whole pear was considered as RoI with an average spectrum. It is worth noting that the hyperspectral data was collected from fixed posture with human involvement, and the selection of the RoI was also manual, using software. It can be seen from the above literature that the manual RoI selection artificially avoids the pedicel or calyx, which is only suitable for laboratory research. These manual RoI selections raise the issue of accuracy and indicate practical application gaps in an assembly line.

This study proposes an automatic method for RoI selection of hyperspectral images in apples with random positions. A non-destructive testing was established and the actual measurement and verification analysis were carried out to evaluate the correctness and effectiveness of the proposed method. Apple sugar contents were determined as a reference study for the automatic detection on the sorting line.

2 Materials and methods

2.1 Experiment material

A total of 135 Yantai Fuji apples of different sizes, shapes, and colors (slice red and striped red) were randomly purchased from the market. Before testing, apples were placed in the laboratory environment for 12 h. After reaching room temperature, all samples were washed to remove surface dirt and dried with blotting papers.

2.2 Equipment and instruments

2.2.1 Sorting line

The sorting line setup is shown in Figure 1, containing different parts such as an apple loading unit, conveying unit, flip device, machine vision unit, hyperspectral imaging system, sorting channel, control unit, and computer processing unit.

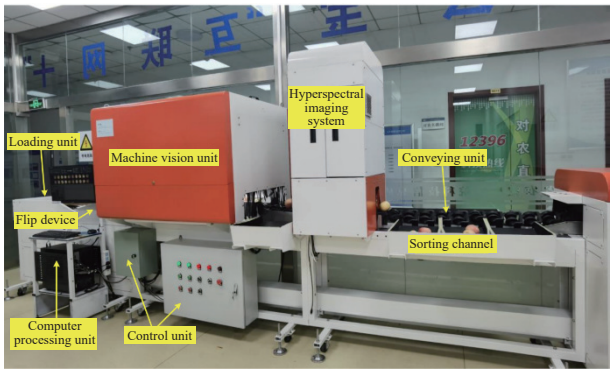

Figure 1 Physical photo of apple sorting line with the hyperspectral imaging system

2.2.2 Hyperspectral imaging system

The schematic diagram of the hyperspectral imaging system used in this research is shown in Figure 2, which includes an imaging spectrometer (Pika XC2, Resonon, Bozeman, United States), lens (focal length of 23 mm), data acquisition software, mobile platform, and a pair of 100 W halogen lamp cups (JCR 12 V 100 W BAU, Ushio, Tokyo, Japan). Light sources are controlled by a power supply switch.

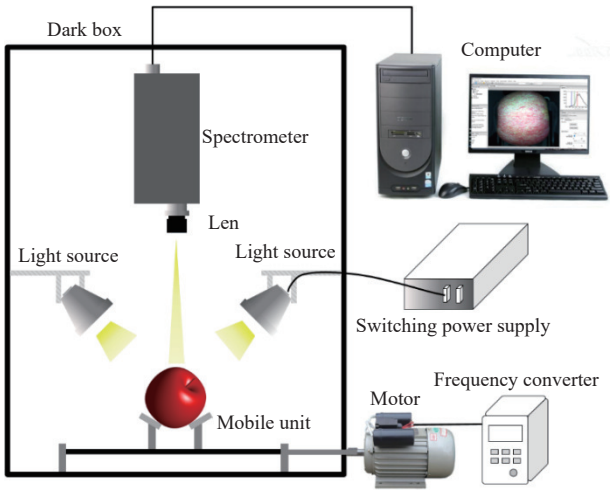

a. Schematic diagram

b. Internal photo

Figure 2 Schematic diagram of the structure and internal photo of the hyperspectral imaging system

An imaging spectrometer was used for real-time hyperspectral image acquisition and adopted the line-scanning method. The parameters of the image acquisition system were 400-1000 nm spectral range with 1.3 nm spectral resolution, 462 spectral channels, 1600 spatial channels, and a maximum of 165 frames/s with 12 bits depth. In order to avoid the influence of surrounding stray light, the imaging spectrometer, lens, light source, and mobile device were placed in a dark box.

2.2.3 Brix meter

Apple sugar contents were measured by using an LH-B55 digital refractometer manufactured by Hangzhou Luheng Biological Technology Co., Ltd, China. The Brix measuring range of the device was 0.0-55.0 with 0.1 resolution.

2.3 Data acquisition

2.3.1 Hyperspectral image data acquisition

The hyperspectral imaging system was used to collect data as shown in Figure 2. The sample exposure time to the imaging

spectrometer was set at 5.5 ms with a 150 Hz frame rate and 0 gain. The light source was turned on for 20 min before capturing the dark-field hyperspectral images, and reflection data was collected followed by black-and-white correction. Afterward, apples were placed in fruit cups on the mobile unit and passed through the imaging spectrometer with random poses, where spectral data of 135 images was obtained using self-written software.

2.3.2 Brix data collection

Apples were sliced at 10 mm thickness using a knife from every 90° angle of the central location of captured images. Furthermore, the peel (Figure 3(1)) was removed and cut into 20 mm-thick cubes (Figure 3(3)). Four cubes (Figure 3(2)) were blended in a manual juicer to obtain 5 mL juice. Brix was determined with an LH-B55 digital refractometer with triplicate measurements by averaging the three data.

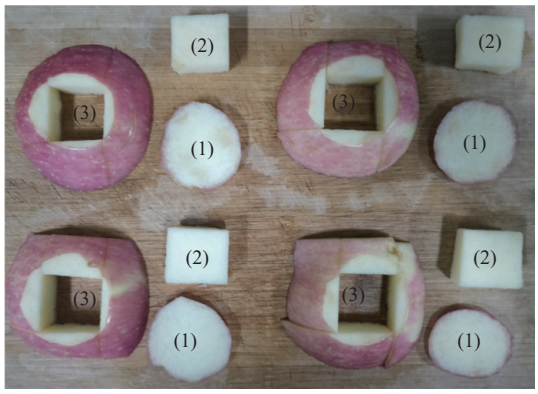

Figure 3 Apple pulp selection area for the Brix data collection

2.4 RoI selection

It can be observed from Figure 4 that the apple occupies only a central area. Based on the maximum horizontal distance of the largest apple among all samples, any area beyond 450 pixels from the horizontal center point is directly discarded, retaining only the central 900-pixel region.

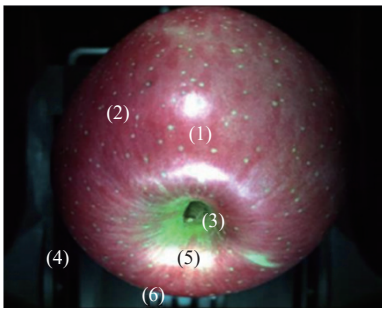

Note: (1) Central region of the apple with high spectral intensity; (2) Apple edge region with low spectral intensity; (3) Apple pedicel region; (4) Normal background area; (5) Overexposed area of apple; (6) Highly reflective areas in the background.

Figure 4 Display of six different regions of hyperspectral images on an apple

The selection of RoI involves choosing a target area within the apple region of the collected hyperspectral image so that it represents the spectral information of the entire apple. Due to the curvature of the apple's surface, the spectral intensity is higher in the central area of the apple and lower around the edges. The spectral curves of different regions in the hyperspectral image exhibit distinct characteristics as shown in Figure 5. These characteristics were the basis of the selection of RoI.

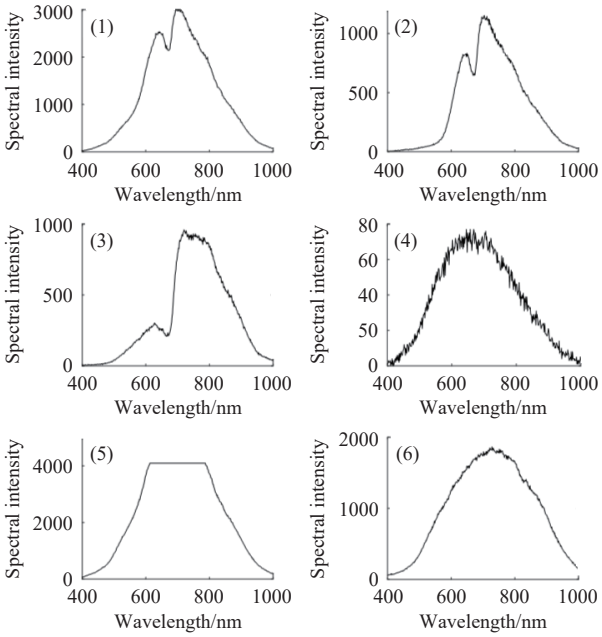

Note: (1) Regions with high spectral intensity; (2) Low spectral intensity; (3) Pedicel; (4) Background; (5) Overexposed; (6) Highly reflective areas in the background.

Figure 5 Spectral curves of the six different regions

2.4.1 Principles for RoI selection

RoI must be of smaller size for the assurance of operation speed and region with higher spectral intensity and signal-to-noise ratio. For the improvement of model stability, it is necessary to eliminate the pedicel and calyx regions to avoid complex structure interruption and variation of spectral curves of normal tissues. Additionally, time spent on the RoI selection method should be less due to the large amount of hyperspectral image data.

2.4.2 RoI selection process

According to the above principles, the selection process of apple RoI is as follows:

Step 1: Threshold segmentation: the spectral curves feature of six different regions shown in Figure 4 demonstrates that maximum spectral intensity approached near 700 nm. Therefore, the spectral intensity of each pixel at 700 nm is used for the threshold segmentation.

Step 2: Morphological etching: the histogram of each pixel of the hyperspectral image was calculated at 700 nm and the relationship between spectral intensity values of each pixel was determined. The pixels with low intensity were removed, and a morphological etching function was performed to remove the areas of high reflection such as pedicel, calyx, and background.

Step 3: Spectral intensity screening: The area (5) in Figure 4 showed high spectral intensity approaching the maximum range of 4095 of the spectrometer, which required elimination owing to a negative impact on spectral data accuracy. Big apple size and more shining skin were the two main factors that generated high reflection. Spectral intensity screening was performed at 700 nm to eliminate higher reflection and specify the area overexposed when intensity was greater than 3900. (The maximum value 4095 was found near 700 nm, not exactly at 700 nm but maybe at 710 nm or 690 nm, so 3900 was selected as the overexposed spectral intensity threshold, with 195 buffs.)

Step 4: After that, to achieve RoI, a histogram of pixels was calculated about spectral intensity value at 700 nm wavelength. The pixel point sets for the first 10%, 20%, 30%, 40%, 50%, 60%, 70%,

80%, 90%, and 100% of the spectral intensity. The partial least squares regression (PLSR) prediction models were established for RoIs of different sizes. During PLSR prediction model development, black-and-white correction of hyperspectral data was carried out for the pixels in RoI, and the average spectrum was calculated as the characteristic spectrum of the apple. Further, the dataset was divided into calibration and test sets at a ratio of 3:1 by the sample partition method based on the joint *X-Y* distance. However, the PLSR model between characteristic spectrum and sugar content was established in the calibration set. Finally, the characteristic spectrum of the test set used in the established model, and predicted sugar contents were obtained. The prediction accuracy was further used as the basis for the selection of the final RoI size.

2.5 Model establishment

The imaging spectrometer possessed 1600 sampling points per frame and 462 wavelengths of data. For this study, an average of 750 frames were obtained with a hyperspectral image size of 1600×462×750 pixels. Hyperspectral image data size was about 1 GB by considering 12 bits depth, and one spectrum covered the space of up to 2 bytes. Raw data has high computational complexity and affects speed and accuracy in model development, though the average spectrum of RoI was used as the characteristic spectra in the prediction model.

2.5.1 Black-and-white correction of RoI

After the selection of the RoI of the apple, the signal-to-noise ratio was improved through the elimination of the influence of noise caused by dark current, background light, and uneven distribution of light sources[18]. The black-and-white correction was performed in two steps to overcome noise. In one step, image of the standard white positive plate (thermoplastic resin) with 99% reflection was observed to obtain full white standard image *W*. At a later stage, the light source was turned off and the lens was attached for the collection of the full black calibration image *D*[19]. The black-and-white correction formula is Equation (1).

$$R_{\lambda,n} = \frac{S_{\lambda,n} - D_{\lambda,n}}{W_{\lambda,n} - D_{\lambda,n}} \times 10\,000 \quad (1)$$

where, $R_{\lambda,n}$, $S_{\lambda,n}$, and $D_{\lambda,n}$ represent the corrected, original, and dark-field hyperspectral data, respectively. $W_{\lambda,n}$ is the total reflection, while subscript λ and n are the n^{th} pixel at λ wavelength.

2.5.2 Spectral data preprocessing

Various noise signals were observed in collected hyperspectral image data due to instrumental electric noise, vibration, stray light of the surrounding environment, and differences in apple shape. The noise signal reduction was necessary for the improvement in the stability of the regression model[20]. In this study, several common spectral preprocessing methods were used for comparative analysis, including standardization, centralization, Savitzky-Golay (S-G) polynomial convolution[21], first-order derivative (D1), multiplicative scatter correction (MSC)[22], and standard normal variation (SNV)[23].

2.5.3 Characteristic band extraction

High resolution of spectral data produces multiple dimension bands and a significant correlation between bands and redundancy. The model was built with full bands and affected the prediction accuracy with complex calculations. Therefore, extraction of featured waveband data was required for the improvement of calculation time and prediction accuracy[24]. Five methods, including successive projection algorithm (SPA)[16,25-27], principal component analysis (PCA)[28,29], backward interval partial least squares (BiPLS)[30], ant colony optimization (ACO)[31], and competitive adaptive reweighting sampling (CARS)[32] were used to extract the characteristic band data and compare the extraction effects.

2.5.4 Model establishment

PLSR is a multiple linear regression algorithm and is especially suited for datasets with more variables than samples[33]. It was first used for the processing of hyperspectral data by Martens and Jensen in 1983[34]. Nowadays it is one of the most used regression algorithms in hyperspectral imaging and has been commonly applied to develop accurate models in predicting properties or composition parameters from hyperspectral data[35]. In this study, five related PLSR models were established and contrasted to obtain the optimal model.

3 Results and discussion

3.1 Selection of original RoI

Experimental results showed that pedicle or calyx and background bright spot regions were efficiently removed with the selection of the first 40% of pixels with high spectral intensity and eliminated 60% of pixels with low spectral intensity. Simultaneously, regions with low spectral intensity and background were removed. The threshold value of spectral intensity above 3900 at 700 nm was used to remove the overexposed region. In this method, two simple and fast threshold segmentation and one etching operation were performed to select the RoI, as shown in Figure 6.

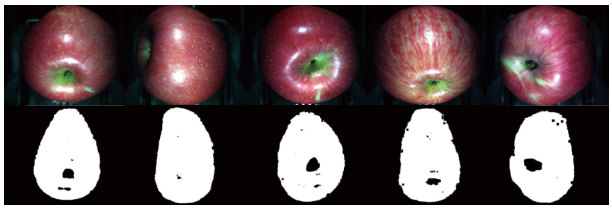

Figure 6 Mask of selected apple's original RoI

3.2 Influence of different RoI sizes on the accuracy of the model

The pixel mask of the first 10%, 20%, 30%, 40%, 50%, 60%, 70%, 80%, 90%, and 100% of spectral intensity values in the original RoI of apple are shown in Figure 7.

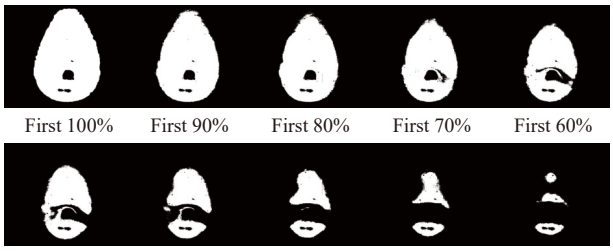

Figure 7 Mask of RoI with different sizes

PLSR prediction model was established with different RoI sizes and RMSEP trend of test set, as shown in Figure 8. An inversely proportional relation was observed between RMSEP and RoI, while prediction error decreased with increment of region size. The higher RoI size provided more spectral information of the whole apple, which led to reduction in RMSEP. However, the first 70% of original RoI generated lowest RMSEP, and no significant changes were observed with the selection of high regions. This phenomenon occurred due to the noise data in RoI. Therefore, the first 70% of the spectral intensity value in the original RoI was considered as the final RoI, and average spectrum of this data was further used for model development.

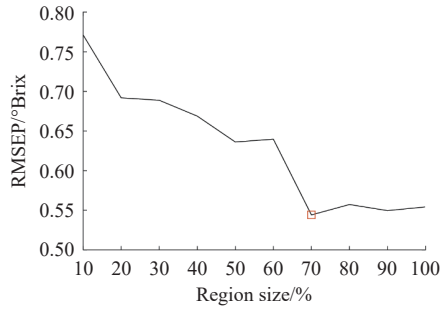

Note: Lowest RMSEP occurred at first 70% of original RoI and no significant changes with the selection of high regions.

Figure 8 RMSEP variation trend of PLSR model with different RoI sizes

3.3 Removal of abnormal samples and sample set division

3.3.1 Removal of abnormal samples

There were chances of irregular patterns of collected hyperspectral data or apple sugar content due to human errors. However, the change in the surrounding environment and instrument can also affect the accuracy of the final model. Therefore, abnormal data should be rejected before modeling. Monte Carlo cross-validation (MCCV) reduces the risks caused by the masking effect and effectively identifies an abnormal lattice along with the spectral array and feature array. It has a greater ability to identify abnormal samples than traditional methods[36]. So, MCCV elimination method was used in this study[37]. In the model development, data was randomly divided into 80% and 20% in calibration and test sets, respectively. A set of predictive values for each sample was obtained after 2000 cycles to calculate the parameters such as mean value (Mean) and standard deviation (STD), as presented in Figure 9. The mean and STD thresholds were 1.5 and 0.5, respectively, while samples with higher mean values were rejected. A total of 11 abnormal samples at No.5, 11, 22, 26, 45, 54, 55, 59, 61, 111, and 112 were rejected, and analysis was performed with the remaining 124 samples.

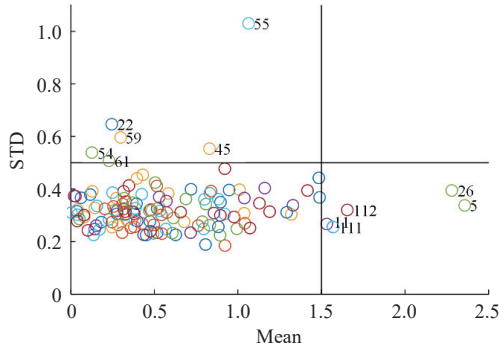

Figure 9 Mean-STD diagram (No. 5, 11, 22, 26, 45, 54, 55, 59, 61, 111, and 112 are not within the threshold)

3.3.2 Sample set division

The total 124 samples were divided into calibration and test sets with a 3:1 ratio by Sample Set Partitioning based on the Joint X-Y Distance (SPXY) method. The distribution of sugar content data is listed in Table 1. It can be seen that the maximum and minimum sugar contents were included in both datasets, and the STD of the test set was less than the calibration set, which expressed proper data division.

3.4 Selection of preprocessing methods for hyperspectral data

The image acquisition system has a 400-1000 nm spectral range with 462 bands. The reflection data on both ends were removed due to the lower intensity and signal-to-noise ratio. Therefore, 387 bands were used with a range of 436-940 nm in this study. Furthermore, the original data was preprocessed by standardization, decentralization, S-G polynomial convolution (second-order 33 points, which is the optimal value of many experiments), first-order derivative, multiple scattering correction (MSC), and standard normal variate (SNV), respectively. The results in Table 2 show that SNV achieved the lowest RMSEP and highest prediction accuracy and was able to effectively remove the noise signal. Therefore, the SNV method was selected to preprocess the spectral data.

Table 1 Sugar content data distribution of calibration set and test set

Sample set	Quantity	Minimum/ °Brix	Maximum/ °Brix	Mean/ °Brix	STD/ °Brix
Calibration set	93	7.6000	14.9000	12.1271	1.5812
Test set	31	9.0000	14.6000	12.2785	1.3699
Total	124	7.6000	14.9000	12.1649	1.5271

Table 2 Influence of different preprocessing methods of hyperspectral data on model accuracy

Pretreatment method	Number of variables	R_{cv}	RMSECV/ °Brix	R_p	RMSEP/ °Brix
Untreated	31	0.8708	0.7829	0.8465	0.6821
Standardized	21	0.9250	0.6050	0.8513	0.6722
Decentralized	27	0.9304	0.5836	0.8703	0.6310
S-G Convolution	32	0.8869	0.7356	0.8000	0.7686
D1	18	0.7913	0.9737	0.8198	0.7335
MSC	27	0.9317	0.5786	0.8749	0.6204
SNV	**27**	**0.9305**	**0.5833**	**0.8785**	**0.6119**

Note: D1: First-order derivative; MSC: Multiplicative scatter correction; and SNV: Standard normal variation.

3.5 Analysis on the selection results of characteristic bands by different methods

3.5.1 Successive projection algorithm (SPA)

SPA is a forward characteristic band selection method that can minimize the collinearity between selected variables by using simple operations in vector space. During input calibration of the dataset into SPA, the maximum number of extracted bands were adjusted up to 30 and were used to analyze the change in root mean square error of cross-validation (RMSECV) with the selected characteristic bands. The results in Figure 10 show that RMSECV approached to minimum with 19 selected bands. The selected characteristic band is shown in Figure 11.

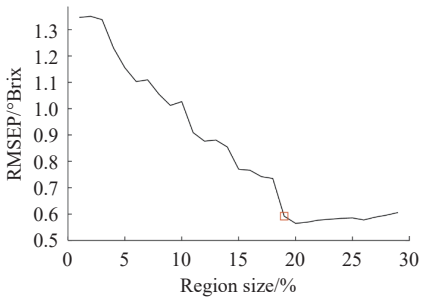

Figure 10 RMSECV variation trend of SPA with the number of selected characteristic bands: RMSECV approached the minimum with 19 selected bands

3.5.2 Principal component analysis (PCA)

PCA provides a data dimensional reduction technique to simplify a large number of related variables. Additionally, this

method optimizes the analysis process and determines the data potential relationship by selecting a few features[38]. PCA can project the original high-dimensional data into low-dimensional characteristic space to select comprehensive variables[26]. In this algorithm, the number k of the extracted principal components was essential. A small k value will affect the extracted principal components by losing some important information in the original hyperspectral data. Similarly, a larger k value causes a failure to reduce the amount of required computation and results in a high number of principal components. However, Figure 12 presents the changing trend of RMSECV and graphs show a gradual decrease in RMSECV with the increment of k. A non-significant change was found in RMSECV as the k reached 41 and increased model calculation complexity. Finally, 41 principal components were selected with a cumulative contribution rate greater than 99%.

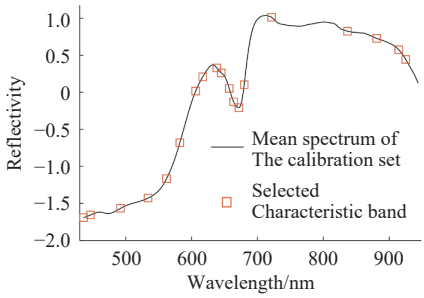

Figure 11 Characteristic band distribution selected by SPA

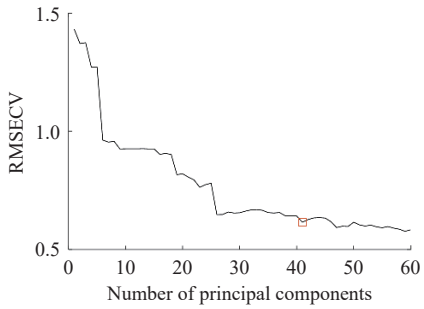

Figure 12 RMSECV variation trend with the number of principal components in PCA: RMSECV with no significant change when the number is larger than 41

3.5.3 Backward interval partial least square (BiPLS)

BiPLS divides the whole band and selects the most representative spectral intervals combination. It is very important to determine the number of subintervals in the BiPLS algorithm which directly affect the accuracy of subsequent models. Therefore, this study set a total of 12 values from 5 to 60 subintervals with an increment of 5. RMSECV variation analysis in relation to different subintervals (Figure 13) demonstrated the lowest values at 25th interval. Removal of subintervals was performed for the optimization. Figure 14 demonstrates that initially, RMSECV tends to decrease, while an increasing trend was found at a later stage with the increment of the number of removed subintervals, and removing 17 subintervals resulted in the lowest RMSECV. However, the remaining 8 subintervals of the No.11, 13, 15, 16, 18, 20, 22, and 24 were finalized, and band distribution is shown in Figure 15.

3.5.4 Ant colony algorithm (ACO)

ACO is defined as a probabilistic algorithm for optimization and possesses the characteristics of information positive feedback distributed computing and heuristic search[30]. The application of ACO in screening characteristic bands is required to determine hyperparameters in the algorithm through multiple experiments. Therefore, the maximum number of iterations, population size, selected bands, volatilization, and significant factor were set as 50, 40, 50, 0.65, and 0.01, respectively. Figure 16 shows the arrangement of the selected frequency of each targeted band. Furthermore, the PLSR model was applied to the first 60 bands and found RMSECV at the minimum level for the first 38 bands. Therefore, these 38 bands were selected as characteristic bands, and their distribution on the spectral curve is shown in Figure 17.

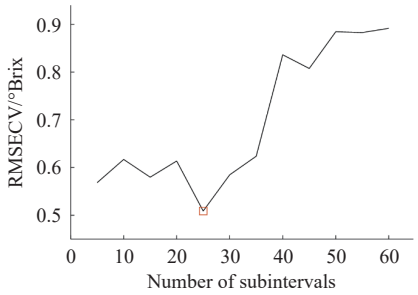

Figure 13 RMSECV variation trend with the number of subintervals in BiPLS: lowest RMSECV at 25th interval

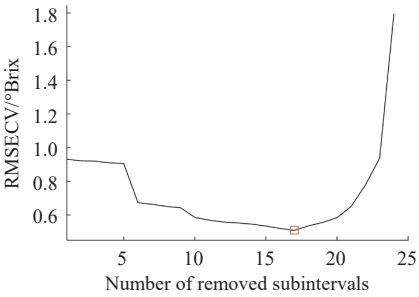

Figure 14 RMSECV variation trend with the number of removed subintervals: lowest RMSECV after removing 17 subintervals

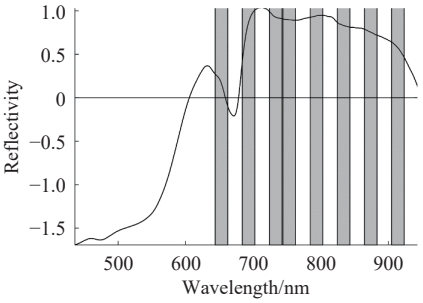

Figure 15 Distribution of BiPLS final selected subintervals

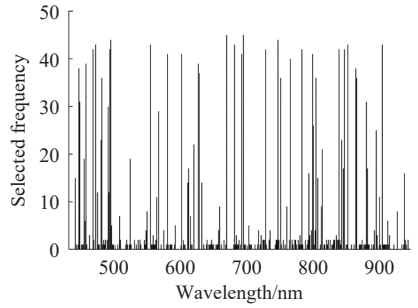

Figure 16 Selected frequency distribution of bands in ACO

3.5.5 Competitive adaptive reweighted sampling algorithm (CARS)

The CARS method can effectively use the regression coefficient of PLSR to select the optimal band combination in the

whole spectrum. The calibration dataset adopted the CARS algorithm and adjusted the maximum number of iterations up to 100 for the characteristic band. The results in Figure 18 show a rapid decreasing trend in the number of retained bands with the increasing iterations. This was due to the rough selection performance at the early stage followed by fine selection. At the 20th cycle sampling, RMSECV reached the lowest value with 40 reserved bands selected as characteristic bands, and the distribution is shown in Figure 19.

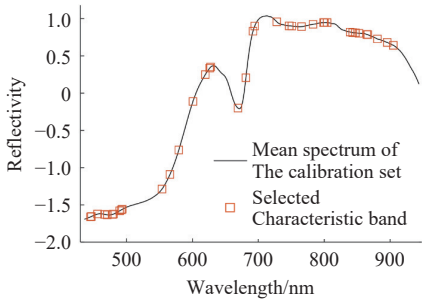

Figure 17 Characteristic band distribution selected by ACO

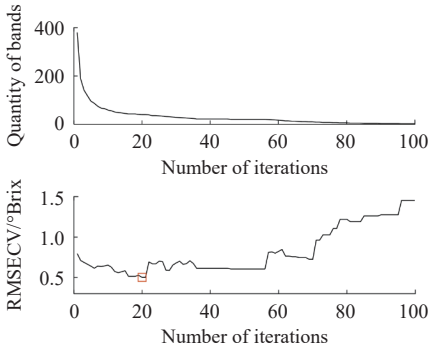

Figure 18 Variation trend of the quantity of bands and RMSECV with the number of iterations in CARS

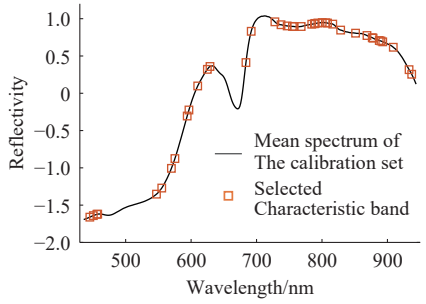

Figure 19 Distribution of characteristic bands selected by CARS

3.5.6 Establishment of regression model and selection of optimal model

After SNV preprocessing, the five methods of SPA, PCA, BiPLS, ACO, and CARS were used to extract characteristic bands for 436-940 nm hyperspectral data and establish the related regression models of SPA-PLSR, PCA-PLSR, BiPLS-PLSR, ACO-PLSR, and CARS-PLSR. A full-spectrum regression model was established to compare the advantages and disadvantages according to prediction results. The results in Table 3 describe that all models achieved higher prediction accuracy except SPA-PLSR. However, slightly higher prediction accuracy was observed in PCA-PLSR and BiPLS-PLSR with comparison of full-spectrum FS-PLSR, and the prediction accuracy of ACO-PLSR was also improved. CARS-PLSR model showed the highest prediction accuracy and best stability and obtained 5.95% higher R_p and 23.50% lower RMSECV by comparing with FS-PLSR. In addition, the CARS-PLSR model reduced the original 380 to 40 dimensions, eliminated maximum redundant information, significantly reduced the computational complexity, and improved the calculation speed.

Table 3 Prediction results of the PLSR model on different numbers of variables

Model name	Number of variables	R_{cv}	RMSECV/ °Brix	R_p	RMSEP/ °Brix
FS-PLSR	27	0.9305	0.5833	0.8785	0.6119
SPA-PLSR	17	0.9327	0.5744	0.8303	0.7139
PCA-PLSR	27	0.9223	0.6154	0.8879	0.5894
BiPLS-PLSR	16	0.9499	0.4976	0.8943	0.5733
ACO-PLSR	23	0.9645	0.4205	0.9056	0.5432
CARS-PLSR	**24**	**0.9595**	**0.3203**	**0.9308**	**0.4681**

In this study, a method was established for the selection of RoI of apple during the application of hyperspectral imaging. After black-and-white correction, spectral data processing and removal of abnormal samples were performed by SNV and MCCV methods, respectively. CARS algorithm was used to extract the characteristic bands, and the PLSR model was applied for prediction of apple sugar content. The determination coefficient R_{cv} and RMSECV of cross-validation were 0.9595 and 0.3203°Brix, respectively. The determination coefficient R_p and RMSEP of prediction value with higher accuracy were 0.9308 and 0.468°Brix, respectively. The predicted apple sugar content and the scatter plots of measured value in calibration and test sets are shown in Figures 20 and 21.

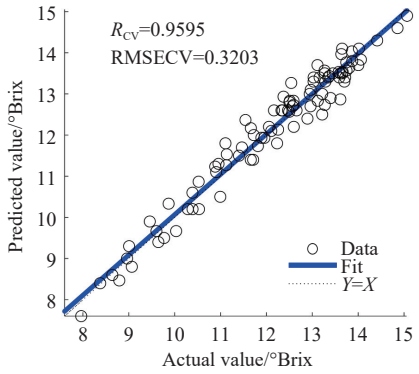

Figure 20 Scatter plot of calibration set prediction results

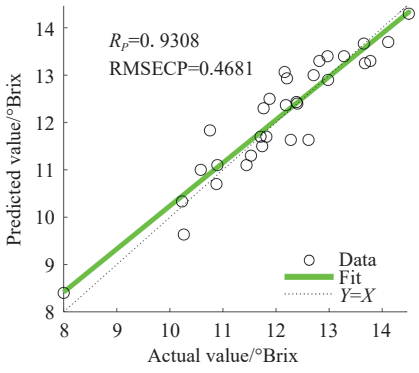

Figure 21 Scatter plot of test set prediction results

4 Conclusions

This study proposed an online RoI selection strategy in a hyperspectral imaging system of random-passed apples. The method showed a significant difference as compared to the manual selection of RoI of fixed-position apple and was found most suitable in sorting line automation. The RoI selection method reduced the time consumption and investigation cost of internal quality inspection.

The first 40% spectral intensity at 700 nm of each pixel was used for threshold segmentation, and intensity optimization was achieved through the removal of variation-causing areas. The PLSR model performed well with the first 70% of RoI for non-destructive prediction of sugar contents. SPXY method was used to divide 124 samples into calibration and prediction sets in a 3:1 ratio. Minimum and maximum sugar contents in the calibration set were 7.6000 and 14.9000, while in the test set they were 9.0000 and 14.6000, respectively. Among all preprocessing methods, SNV demonstrated the best efficiency and obtained 0.8785 R_p and 0.6119°Brix RMSEP followed by MSC. The characteristic bands were extracted through the CARS algorithm, and the PLSR model was used for the prediction of sugar content. The model performed well with high accuracy and obtained 0.9595 of R_{cv} and 0.3203°Brix of RMSECV. However, efficient prediction capability exhibited high R_p and low RMSEP, at about 0.9308 and 0.4681°Brix, respectively. CARS-PLSR also showed the best stability and obtained 5.95% higher R_p and 23.50% lower RMSECV compared to FS-PLSR. Moreover, the established model was highly stable, with less computational complexity and fast calculation speed. RoI selection is a promising approach and provides a theoretical foundation to design an online apple grading system with hyperspectral imaging technology.

Acknowledgements

This work was financially supported by Shandong Provincial Natural Science Foundation, China (Grant No. ZR2022MC067); the National Key R&D Program of China (Grant No. 2021YFB3901303); the Key R&D Program of Shandong Province, China (Grant No. 2022 CXGC010610); the Agricultural Scientific and Technological Innovation Project of Shandong Academy of Agricultural Sciences, China (Grant No. CXGC2023D02); and the Special International Cooperation Program of Shandong Academy of Agricultural Sciences, China (Grant No. CXGC2023G24).

[References]

[1] Ferrari C, Foca G, Calvini R, Ulrici A. Fast exploration and classification of large hyperspectral image datasets for early bruise detection on apples. Chemometrics and Intelligent Laboratory Systems, 2015; 146: 108–119.

[2] Chen H Z, Qiao H L, Lin B, Xu G L, Tang G Q, Cai K. Study of modeling optimization for hyperspectral imaging quantitative determination of naringin content in pomelo peel. Computers and Electronics in Agriculture, 2019; 157: 410–416.

[3] Tian H, Wang S, Xu H R, Ying Y B. Modeling method for SSC prediction in pomelo using Vis-NIRS with wavelength selection and latent variable updating. Int J Agric & Biol Eng, 2024; 17(1): 251–260.

[4] Wei Q Q, Zheng Y R, Chen Z Q, Huang Y, Chen C Q, Wei Z B, et al. Nondestructive perception of potato quality in actual online production based on cross-modal technology. Int J Agric & Biol Eng, 2023; 16(6): 280–290.

[5] Chithra P, Henila M. Apple fruit sorting using novel thresholding and area calculation algorithms. Soft Computing, 2021; 25(1): 431–445.

[6] Martins J A, Guerra R, Pires R, Antunes M D, Panagopoulos T, Br´azio A, et al. SpectraNet–53: A deep residual learning architecture for predicting soluble solids content with VIS-NIR spectroscopy. Computers and Electronics in Agriculture, 2022; 197: 106945.

[7] Tian S J, Wang S, Xu H R. Early detection of freezing damage in oranges by online Vis/NIR transmission coupled with diameter correction method and deep 1D-CNN. Computers and Electronics in Agriculture, 2022; 193: 106638.

[8] Wu G S, Fang Y L, Jiang Q Y, Cui M, Li N, Ou Y M, et al. Early identification of strawberry leaves disease utilizing hyperspectral imaging combing with spectral features, multiple vegetation indices and textural features. Computers and Electronics in Agriculture, 2023; 204: 107553.

[9] Xu H L, Sun Y X, Cao X L, Ji C M, Chen L, Wang H Y. Apple quality detection based on photon transmission simulation and convolutional neural network. Transactions of the CSAM, 2021; 52(8): 338–345. (in Chinese)

[10] Gamal E, Ning W, Clément V. Detecting chilling injury in Red Delicious apple using hyperspectral imaging and neural networks. Postharvest Biology and Technology, 2009; 52(1): 1–8.

[11] Guo Z. Nondestructive detection techniques and devices for assessing quality attributes of apples based on NIR spectroscopy and hyperspectral imaging. Beijing: China Agricultural University, 2015.

[12] Mo C, Kim M, Kim G, Lim J, Delwiche S R, Chao K, et al. Spatial assessment of soluble solid contents on apple slices using hyperspectral imaging. Biosystems Engineering, 2017; 159: 10–21.

[13] Lan W J, Jaillais B, Renard C M G C, Leca A, Chen S C, Le Bourvellec C, et al. A method using near infrared hyperspectral imaging to highlight the internal quality of apple fruit slices. Postharvest Biology and Technology, 2021; 175: 111497.

[14] Che W K, Sun L J, Zhang Q, Tan W Y, Ye D D, Zhang D, et al. Pixel based bruise region extraction of apple using Vis-NIR hyperspectral imaging. Computers and Electronics in Agriculture, 2018; 146: 12–21.

[15] Zha Q M. Research on nondestructive testing of hardness, moisture and soluble solids content of apple based on hyperspectral imaging technology. MS dissertation. Nanjing: Nanjing Agricultural University, 2017; 81p. (in Chinese)

[16] Feng D, Ji J W, Zhang L, Liu S J, Tian Y W. Optimal wavelengths extraction of apple brix and firmness based on hyperspectral imaging. Chinese Journal of Luminescence, 2017; 38(6): 799–806. (in Chinese)

[17] Xu L. Detection of soluble solids content of fruit based on Vis-NIR spectroscopy and imaging technology. MS dissertation. Hefei: Anhui University, 2019; 74p. (in Chinese)

[18] Wang F Y, Zheng J Y, Ruan H J, Yuan X L. Research on non-destructive prediction model of sugar content of bagged and non-bagged apples based on hyperspectrum. Shandong Agricultural Sciences, 2020; 52(6): 129–136. (in Chinese)

[19] Ma H L, Wang R L, Cai C, Wang D. Rapid identification of apple varieties based on hyperspectral imaging. Transactions of the CSAM, 2017; 48(4): 305–312. (in Chinese)

[20] Zhou Y, Dai S G, Lyu J, Liu T B, Shi Y. Effect of spectral pretreatment on near infrared spectroscopy for rapid detection of wine alcohol. Opto-Electronic Engineering, 2011; 38(4): 54–58. (in Chinese)

[21] Savitzky A, Golay M J E. Smoothing and differentiation of data by simplified least squares procedures. Analytical Chemistry, 1964; 36(8): 1627–1639.

[22] Isaksson T, Naes T. The effect of multiplicative scatter correction (MSC) and linearity improvement in NIR spectroscopy. Applied Spectroscopy, 1988; 42(7): 1273–1284.

[23] Barnes R J, Dhanoa M S, Lister S J. Standard normal variate transformation and de-trending of near-infrared diffuse reflectance spectra. Applied Spectroscopy, 1989; 43(5): 772–777.

[24] Liu T. New wavelengths selection method for molecular spectra based on Ant Colony optimization and fundamental applications. Master dissertation. Hangzhou: Zhejiang University, 2017; 123p.

[25] Araújo M C U, Saldanha T C B, Galvão R K H, Yoneyama T, Visani V. The successive projections algorithm for variable selection in spectroscopic multicomponent analysis. Chemometrics and Intelligent Laboratory Systems, 2001; 57(2): 65–73.

[26] Wang J X, Liu X M, Liu S X, Quan Z K, Xu C B, Jiang H. Prediction of nitrogen content in apple leaves in each growth period based on combined color characteristics. Transactions of the CSAM, 2021; 52(10): 272–281. (in Chinese)

[27] Liu Y D, Xiao H C, Sun X D, Zhu D N, Han R B, Ye L Y, et al. Spectral feature selection and discriminant model building for citrus leaf Huang-longbing. Transactions of the CSAE, 2018; 34(3): 180–187. (in Chinese)

[28] Shahin M A, Symons S J. Detection of *Fusarium* damaged kernels in Canada Western Red Spring wheat using visible/near-infrared hyperspectral imaging and principal component analysis. Computers and Electronics in Agriculture, 2011; 75(1): 107–112.

[29] Wang S P, Teng J, Zheng P C, Liu P P, Gong Z M, Gao S W, et al. Optimizing processing pressure of Qingzhuan tea and development of GCG models for near infrared spectroscopy detection. Transactions of the CSAE, 2020; 36(8): 271–277. (in Chinese)

[30] Huang G Q, Duan H W, He J H, Han L J. Rapid quantitative analysis of crop straws' thermal conductivity based on infrared photoacoustic spectroscopy. Transactions of the CSAM, 2018; 49(7): 342–347. (in

Chinese)

[31] Dorigo M, Maniezzo V, Colorni A. Ant system: optimization by a colony of cooperating agents. IEEE Transactions on Systems, Man, and Cybernetics, Part B (Cybernetics), 1996; 26(1): 29–41.

[32] Li J B, Peng Y K, Chen L P, Huang W Q. Near-infrared hyperspectral imaging combined with CARS algorithm to quantitatively determine soluble solids content in "Ya" pear. Spectroscopy and Spectral Analysis, 2014; 34(5): 1264–1269. (in Chinese)

[33] Wold S, Ruhe A, Wold H, Dunn I W J. The collinearity problem in linear regression. The partial least squares (PLS) approach to generalized inverses. SLAM Journal on Scientific & Statistical Computing, 1984; 5(3): 735–743.

[34] Martens H, Jensen S A. Partial least squares regression: a new two stage NIR calibration method. Progress in Cereal Chemistry and Technology, 1983; 607–647.

[35] Borràs E, Ferré J, Boqué R, Mestres M, Aceña L, Busto O. Data fusion methodologies for food and beverage authentication and quality assessment-A review. Analytica Chimica Acta, 2015; 891: 1–14.

[36] Wang F Y, Zhao Y M, Zheng J Y, Qi K K, Fan Y Y, Yuan X L, et al. Estimation model of soluble solids content in bagged and non-bagged apple fruits based on spectral data. Computers and Electronics in Agriculture, 2021; 191: 106492.

[37] Liu C L, Hu Y J, Wu S N, Sun X R, Dou S L, Miao Y Q, et al. Outlier sample eliminating methods for building calibration model of near infrared spectroscopy analysis. Journal of Food Science and Technology, 2014; 32(5): 74–79. (in Chinese)

[38] He L L, Fang W T, Zhao G N, Wu Z C, Fu L S, Li R, et al. Fruit yield prediction and estimation in orchards: A state-of-the-art comprehensive review for both direct and indirect methods. Computers and Electronics in Agriculture, 2022; 195: 106812.